



Optimal probabilistic placement of facilities using a surrogate model for 3D tsunami simulations

Kenta Tozato¹, Shuji Moriguchi², Shinsuke Takase³, Yu Otake¹, Michael R. Motley⁴, Anawat Suppasri², and Kenjiro Terada²

¹Department of Civil and Environmental Engineering, Tohoku University, Aza-Aoba 6-6-06, Aramaki, Aoba-ku, Sendai 980-8579, Japan

²International Research Institute of Disaster Science, Tohoku University, Aza-Aoba 468-1, Aramaki, Aoba-ku, Sendai 980-8572, Japan

³Department of Civil Engineering and Architecture, Hachinohe Institute of Technology, 88-1 Ohbiraki, Myo, Hachinohe, Aomori 031-8501, Japan

⁴Civil and Environmental Engineering, University of Washington, 201 More Hall, Box 352700, Seattle, Washington, 98195-2700, USA.

Correspondence: Kenta Tozato (kenta.tozato.t2@dc.tohoku.ac.jp)

Abstract. Tsunamis are associated with numerous uncertainties. Therefore, there has been an emphasis on setting the placement of infrastructure facilities based on probabilistic approaches. However, advanced numerical simulations have been often insufficiently utilized due to high computational costs. Therefore, in this study, we developed a framework that could efficiently utilize the information obtained from advanced numerical simulations for probabilistic assessment and investigation of the optimal placement of facilities based on calculated probability. Proper orthogonal decomposition (POD) techniques were employed for utilizing the data from the numerical simulations for probabilistic risk evaluation. We constructed a surrogate model in which POD was efficiently used to extract the spatial modes. The results of the numerical simulation were expressed as a linear combination of the modes, and the POD coefficients were expressed as a function of the uncertainty parameters to represent a result of an arbitrary scenario at a low computational cost. We conducted numerical simulations of the 2011 tsunami off the Pacific Coast caused by Tohoku Earthquake as an example of the method proposed in this study. The tsunami reached the target area, and the fault parameters of “slip” and “rake” were selected as the target uncertainties. We then created several scenarios in which these parameters were changed and conducted further numerical simulations using POD to construct a surrogate model. We selected the maximum inundation depth in the target area and the maximum impact force that acts on the buildings as the target risk indices, and we constructed a surrogate model of the spatial distributions of each indicator. Furthermore, we conducted Monte Carlo simulations using the constructed surrogate model and the information on fluctuations in uncertainties to calculate the spatial distribution of the failure criterion exceedance probabilities. We then used the Monte Carlo simulation results and a genetic algorithm to identify the optimal placement of facilities based on probability. We also discuss how the optimal placement changes according to differences in risk indices and the differences between parallel and series systems. The failure scenarios for each system are also discussed based on the failure probability. We show that the proposed method of efficiently utilizing advanced numerical simulation information was useful for conducting probabilistic hazard assessments and investigating the optimal placement of facilities based on probability theory.



1 Introduction

Numerical analysis techniques for tsunamis have developed considerably over the years, and high-accuracy hazard assessments and predictions have now become possible (Qin et al., 2018; Xiong et al., 2019). Natural disasters such as tsunamis have numerous uncertainties; hence, conducting probabilistic risk assessments that consider such factors is important. However, advanced numerical analyses are generally computationally expensive. Furthermore, they are not very compatible with probabilistic assessments and require multiple trials. Therefore, a framework that can efficiently combine these aspects is required.

Probabilistic risk assessments of disasters have been researched for many years in the seismology fields. Among these, the study by Cornell (Cornell, 1968) is considered groundbreaking. Many research results have been reported on probabilistic seismic hazard analyses (PSHA) (e.g., McGuire, 1977; Ishikawa and Kameda, 1988). Furthermore, probabilistic tsunami hazard analyses (PTHA) have been established based on PSHAs; they have been proposed as a method for understanding the relationship between tsunami heights and exceedance probabilities in a specified period. PTHAs are practical methods for mitigating disaster damage, and many studies on PTHA have been reported (e.g., Annaka et al., 2007; Power et al., 2007; Thio et al., 2007; Mitsoudis et al., 2012; Fukutani et al., 2021, 2015; Park and Cox, 2016); many review papers have also reviewed the topic (Geist and Parsons, 2006; Mori et al., 2017).

Furthermore, the appropriate placement of infrastructure and evacuation facilities is important for minimizing damage due to tsunamis. Numerous studies have used a probabilistic approach for the optimal placement of network systems and facilities by considering the uncertainties of disasters such as earthquakes or tsunamis. Such research examples include risk assessments for infrastructure system networks (Gomez and Baker, 2019; Miller and Baker, 2015), optimization of relief supply bases and their delivery (Cavdur et al., 2020a, b; Maharjan and Hanapla, 2020), optimal placement of public and evacuation facilities (Park et al., 2012; Zhang and Yun, 2019; Doerner et al., 2008), emergency medical service networks (Mohamadi and Yaghoubi, 2017), and optimal allocation of budgets for disaster countermeasures (Rawls and Turnquist, 2010).

Thus, many research examples on the probabilistic hazard assessments of tsunamis and probabilistic optimal placement of facilities exist; however, few studies have sufficiently used the information obtained from advanced numerical analysis. In this study, we applied the theory of mode decomposition using proper orthogonal decomposition (POD) (Kerschen et al., 2005) for solving such issues. The objectives of POD include extracting data characteristics or reducing data dimensions. POD is often treated as an equivalent of Karhunen–Loeve decomposition developed by Karhunen (1947) or Kosambi (1943); or principal component analysis (PCA) (Jolliffe and Cadima, 2016) developed by Hotelling (1933). POD has numerous application examples in a wide range of fields; furthermore, there are various application examples in the fields of seismic engineering and tsunami engineering. For example, Ha et al. (2008) applied POD for reducing computational costs to construct a tsunami surrogate model. LeVeque et al. (2016) and Melgar et al. (2016) applied the Karhunen–Loeve expansion to consider the distribution of fault slips under various scenarios. Furthermore, Nojima et al. (2018) conducted research on the combination of model decomposition based on singular value decomposition and numerical simulations to predict the distribution of strong motion; Bamer and Bucher (2012) used nonlinear finite element methods to construct a surrogate model, using POD for the prediction of the behavior of buildings. Moreover, Fukutani et al. (2021) constructed a surrogate model that used POD to im-



plement probabilistic inundation assessments. POD can extract the features of spatial and temporal distributions of risk indices; thus, it is suitable for the construction of surrogate models for disaster hazard assessment.

Given this context, in this study, we constructed a surrogate model by applying POD to advanced three-dimensional (3D) tsunami simulation results; we propose a method that uses this surrogate model to efficiently investigate the optimal placement of facilities such as infrastructure facilities, relief supply bases, and evacuation shelters based on probability theory. Research examples of probabilistic assessments of tsunami hazards using surrogate models of numerical simulations include the previously mentioned approach of using mode decomposition by Fukutani et al. (2021) and the approach of using response surfaces by Kotani et al. (2020)); however, no research examples exist in which the optimal placement of facilities has been investigated based on probability theory using a surrogate model. Therefore, in this study, we constructed a surrogate model using mode decomposition on information obtained from advanced numerical simulations. Moreover, we proposed a method that could efficiently investigate the optimal placement of facilities based on probability theory using this surrogate model.

The structure of this paper is as follows. In Section 2, the framework and methods used in this study are described. In Section 3, we applied the proposed method to the 2011 Off the Coast of Tohoku Earthquake as an application example that considers the actual damage and verified the validity of the constructed surrogate model; we also implemented Monte Carlo simulations to conduct probabilistic risk assessments. Furthermore, the Monte Carlo simulation results and a genetic algorithm were used to investigate the optimal placement of facilities, and the usefulness of the proposed method was discussed. Finally, Section 4 describes the conclusions.

2 Search method for the probabilistic optimal placement using a surrogate model

The proposed method is described in this section. In this study, a combined two-dimensional (2D) and 3D tsunami analysis was first conducted for multiple scenarios with different fault parameters. The maximum tsunami fluid force and the maximum inundation depth were adopted as the assessment indicators. Next, POD was applied to the results obtained from these analyses to extract the spatial modes of the tsunami fluid force and inundation depth; these spatial modes were used to construct a surrogate model; based on this model, the numerical analysis results of an arbitrary scenario could be calculated within a short time. Furthermore, this surrogate model and uncertainty parameter fluctuation information were combined to implement a Monte Carlo simulation and compute the probability distribution of the tsunami fluid force and inundation depth at each assessment point; a threshold value was set to create an exceedance probability map. Finally, the Monte Carlo simulation results were used, and a genetic algorithm was applied to investigate the optimal facility placement. Fig. 1 shows a flowchart of this study. From the next sub-section, the methods used in each portion are detailed. Of these, for the methods described in Sections 2.1 and 2.2, the methods proposed by Tozato et al. (2022) were adopted.

2.1 Tsunami simulation method

Numerical analyses were first conducted to construct a surrogate model of each indicator in the target region. A numerical analysis that combined 2D and 3D analysis was conducted; first, a wide-area 2D tsunami analysis was conducted, and the time

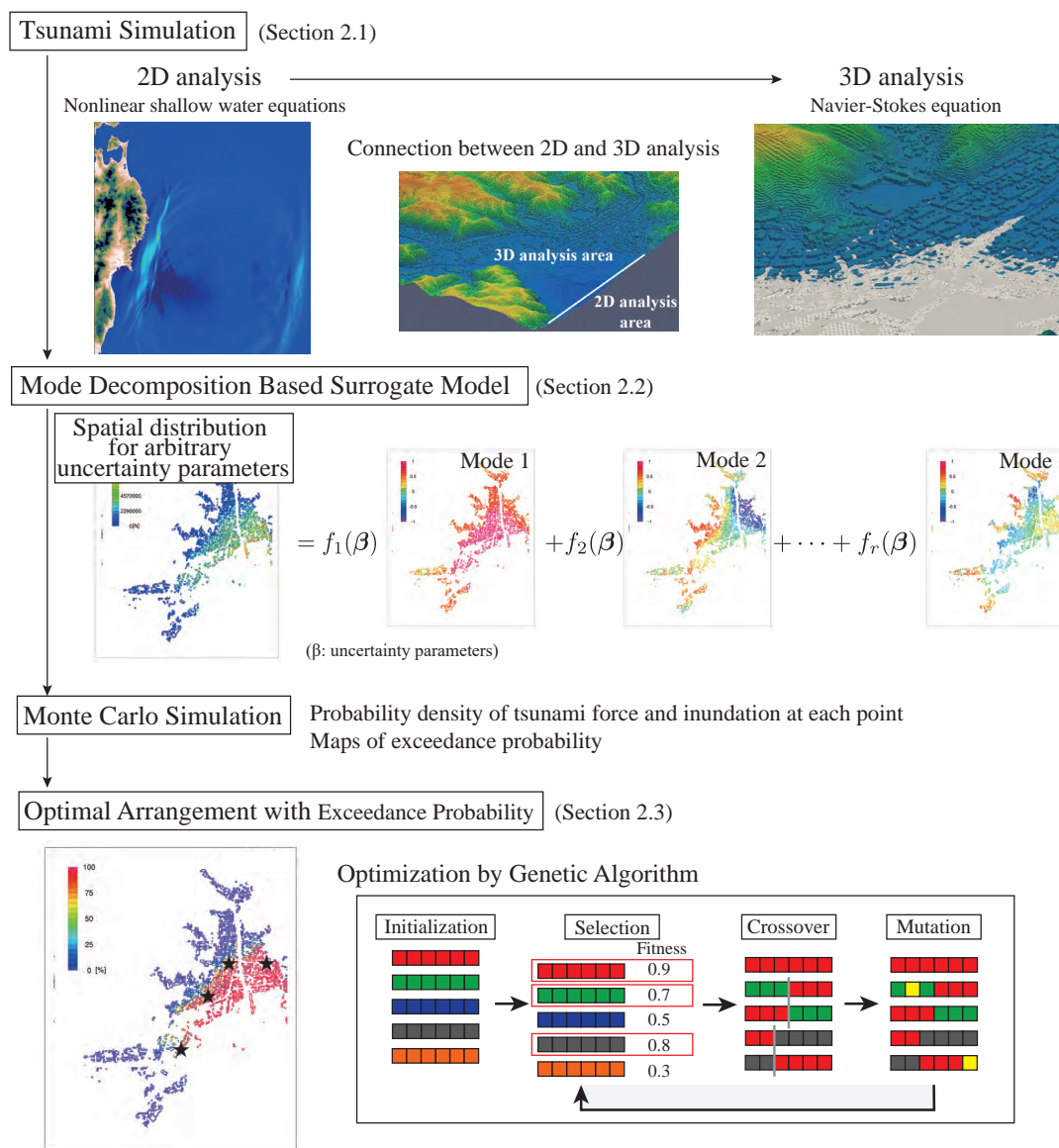


Figure 1. Flowchart of probabilistic tsunami hazard analysis using the mode-decomposition-based surrogate model.



history of the tsunami wave height and flow velocity that were observed offshore of the target area were acquired. In this study, analyses were conducted using TUNAMI-N2 (Imamura, 1995; Goto et al., 1997). The following continuity and nonlinear long
 90 wave equations are solved in the 2D analysis:

$$\frac{\partial \eta}{\partial t} + \frac{\partial M}{\partial x} + \frac{\partial N}{\partial y} = 0 \quad (1)$$

$$\frac{\partial M}{\partial t} + \frac{\partial}{\partial x} \left[\frac{M^2}{D} \right] + \frac{\partial}{\partial y} \left[\frac{MN}{D} \right] + gD \frac{\partial \eta}{\partial x} + \frac{gn^2}{D^{7/3}} N \sqrt{M^2 + N^2} = 0 \quad (2)$$

$$95 \quad \frac{\partial N}{\partial t} + \frac{\partial}{\partial x} \left[\frac{MN}{D} \right] + \frac{\partial}{\partial y} \left[\frac{N^2}{D} \right] + gD \frac{\partial \eta}{\partial y} + \frac{gn^2}{D^{7/3}} M \sqrt{M^2 + N^2} = 0 \quad (3)$$

where M and N are the flow rates in the x and y directions, respectively, η is the water level, D is the total water depth, g is gravitational acceleration and n is the Manning roughness coefficient.

The obtained tsunami wave height and flow velocity were set as the boundary conditions, and the tsunami reaching the target area was analyzed. The time-series data of the wave height and flow velocity obtained from the 2D wide-area analysis
 100 are stored and transferred to the 3D numerical analysis by linear interpolation in space. The interpolated values are given to the 3D analysis as input data.

A 3D analysis was performed in this portion to assess the fluid force acting on the buildings in the target area. We employed the following set of 3D Navier-Stokes and continuity equations in the analysis domain $\Omega_{ns} \in R^3$

$$105 \quad \rho \left(\frac{\partial \mathbf{u}}{\partial t} + \mathbf{u} \cdot \nabla \mathbf{u} - \mathbf{f} \right) - \nabla \cdot \boldsymbol{\sigma} = 0 \quad (4)$$

$$\nabla \cdot \mathbf{u} = 0 \quad (5)$$

where ρ is the mass density, \mathbf{u} is the velocity vector, $\boldsymbol{\sigma}$ is the stress tensor, and \mathbf{f} is the body force vector. Also, assuming a Newtonian fluid, the stress is calculated as

$$\boldsymbol{\sigma} = -p\mathbf{I} + 2\mu\boldsymbol{\varepsilon}(\mathbf{u}) \quad (6)$$

110 where p is the pressure, μ is the coefficient of viscosity, and $\boldsymbol{\varepsilon}(\mathbf{u})$ is the velocity gradient tensor defined as

$$\boldsymbol{\varepsilon}(\mathbf{u}) = \frac{1}{2} (\nabla \mathbf{u} + (\nabla \mathbf{u})^T) \quad (7)$$

To solve the governing equations of the 3D simulation, the stabilized finite element method (SFEM) is used in this study. The method in Takase et al. (2016) was used for the boundary conditions of the 2D and 3D analyses. For the tsunami uncertainty, two fault parameters (described later) were adopted as the uncertainty parameters, and numerical analyses were conducted for
 115 several scenarios in which these parameters were changed. Specific analysis area setting conditions are shown in Section 3.



2.2 Construction of the surrogate model using mode decomposition

Proper orthogonal decomposition (POD) was used to extract the spatial modes in this study. POD can efficiently express data and extract the basis representing data characteristics. To apply POD to the data obtained from numerical analysis, a data matrix was first defined. When data from a given scenario i are set as a vector and defined as \mathbf{x}_i (called a data vector), then the result
 120 of the data vectors corresponding to the number of scenarios arranged in the column direction is defined as follows:

$$\mathbf{X} = \begin{pmatrix} | & & | \\ \mathbf{x}_1 & \cdots & \mathbf{x}_N \\ | & & | \end{pmatrix} \quad (8)$$

Here, N refers to the number of scenarios, and the data vector is defined as a vector with a total of n elements. Furthermore, the vertical line in Eq. (8) was used to indicate that the data vector is a column vector. Using this matrix, the covariance matrix of the data was expressed in the form of $\mathbf{C} = \mathbf{X}\mathbf{X}^T$; the eigenvalues represent the variance, and the eigenvectors represent
 125 the spatial mode (characteristic of the spatial distribution). In this study, we assumed that the eigenvalues were arranged in descending order from the first mode, and the eigenvalue and eigenvector corresponding to the j -th mode were expressed as λ_j and \mathbf{u}_j , respectively. Furthermore, in POD, the contribution rate of each mode is often used as a criterion for determining the number of dimensions to be reduced. The contribution rate is an index that shows how much each mode explains the data, and the contribution rate of the j -th mode is expressed as follows, using the eigenvalues.

$$130 \quad d_j = \frac{\lambda_j}{\sum_{k=1}^n \lambda_k} \quad (9)$$

Furthermore, singular value decomposition was used to express the data matrix as follows using the eigenvalue λ_j and the eigenvector \mathbf{u}_j .

$$\mathbf{X} = \mathbf{U}\mathbf{\Sigma}\mathbf{V}^T = \begin{pmatrix} | & & | \\ \mathbf{u}_1 & \cdots & \mathbf{u}_p \\ | & & | \end{pmatrix} \begin{pmatrix} \sqrt{\lambda_1} & & \\ & \ddots & \\ & & \sqrt{\lambda_p} \end{pmatrix} \begin{pmatrix} - & \mathbf{v}_1 & - \\ & \vdots & \\ - & \mathbf{v}_p & - \end{pmatrix} = \mathbf{U}\mathbf{A} \quad (10)$$

Here, \mathbf{U} is a matrix in which the modes are arranged in the column direction, $\mathbf{\Sigma}$ is a matrix in which the square roots of the
 135 eigenvalues are arranged in diagonal terms, \mathbf{V} is a matrix in which the eigenvectors of $\mathbf{X}^T\mathbf{X}$ are arranged, p is the number of eigenvalues that is greater than zero, and $\mathbf{A} = \mathbf{\Sigma}\mathbf{V}^T$ is a matrix in which the POD coefficients are arranged. The relationship of singular value decomposition for the result of one scenario is given as follows:

$$\mathbf{x}_i = \sum_{k=1}^p \alpha_{ik} \mathbf{u}_k = \alpha_{i1} \mathbf{u}_1 + \cdots + \alpha_{ip} \mathbf{u}_p \quad (11)$$

Here, α_{ik} shows the k -by- i column component of the matrix in which the POD coefficients are arranged. When modes with
 140 low explainability for the data are removed, and the data are expressed in an approximate manner, the number of modes r to be reduced is determined from the contribution rate and other indicators and is expressed as follows as a linear sum excluding



the modes with a low contribution rate.

$$\mathbf{x}_i \simeq \sum_{k=1}^r \alpha_{ik} \mathbf{u}_k = \alpha_{i1} \mathbf{u}_1 + \dots + \alpha_{ir} \mathbf{u}_r \quad (12)$$

145 However, notably, a reduction in dimensions will result in a loss of the information contained in the omitted modes. Here, if this data \mathbf{x}_i is the result of the uncertainty parameter β_i , then the POD coefficient of any uncertainty parameter β can be expressed. Therefore, next, the POD coefficient α_{ik} is expressed as a function $f_k(\beta)$ ($k = 1, \dots, r$) of the input parameter that expresses the uncertainty. The surrogate model can be expressed as follows by expressing this as a function of the uncertainty parameter for each corresponding mode.

$$\hat{\mathbf{x}}(\beta) = \sum_{k=1}^r f_k(\beta) \mathbf{u}_k \quad (13)$$

150 In this study, the radial basis functions (RBF) (Buhmann, 1990) were used as the interpolation functions. RBF interpolation can be used to handle cases where the analysis scenarios are not evenly arranged in the parameter space. The function $f_k(\beta)$ corresponding to mode k can be expressed as follows:

$$f_k(\beta) = \sum_{i=1}^N w_i \phi(\beta, \beta_i) = \sum_{i=1}^N w_i \exp(-\gamma \|\beta - \beta_i\|^2) \quad (k = 1, \dots, r) \quad (14)$$

155 Here, β_i is the input parameter group for scenario i , w_i is the weight, and $\phi(\beta, \beta_i)$ is the basis function; γ is a parameter that determines the smoothness of the function. The weight of RBF interpolation can be obtained in the following form by substituting the correspondence between the known input parameter β_i and the coefficient value α_{ik} that expresses the output result.

$$\begin{pmatrix} \alpha_{1k} \\ \vdots \\ \alpha_{Nk} \end{pmatrix} = \begin{pmatrix} \phi(\beta_1, \beta_1) & \dots & \phi(\beta_1, \beta_N) \\ \vdots & & \vdots \\ \phi(\beta_N, \beta_1) & \dots & \phi(\beta_N, \beta_N) \end{pmatrix} \begin{pmatrix} w_1 \\ \vdots \\ w_N \end{pmatrix} \quad (k = 1, \dots, r) \quad (15)$$

They can be expressed in their respective bold forms as follows:

$$160 \quad \boldsymbol{\alpha}_k = \boldsymbol{\Phi} \mathbf{w}_k \quad (k = 1, \dots, r) \quad (16)$$

Here, $\boldsymbol{\alpha}_k$ is a vector in which the coefficients of the k -th mode are arranged, and \mathbf{w}_k is a vector in which the weights of $f_k(\beta)$ are arranged. The function using the weight obtained in Eq. (15) is expressed as an interpolation passing through all the referenced data points. However, cases in which the referenced data points change or vibrate at a local level can result in an interpolation wherein the accuracy of the physical meaning expression is low. To resolve such issues, we introduced a regularization term when computing the weights. Specifically, we introduced L2 regularization called ridge regression (Hoerl and Kennard, 1970), and weight \mathbf{w}_k was obtained by solving the following optimization problem.

$$\arg \min_{\mathbf{w}_k} (\|\boldsymbol{\alpha}_k - \boldsymbol{\Phi} \mathbf{w}_k\|_2^2 + \lambda \|\mathbf{w}_k\|_2^2) \quad (17)$$



This process is generally used in the field of machine learning to prevent overfitting; λ indicates the degree of regularization. Introducing the regularization term allows for the prevention of local vibrations and enables a smooth interpolation. However, care must be taken for cases in which regularization is introduced because this may not pass through all data points. Furthermore, the accuracy of interpolation depends on the RBF parameter γ and regularization parameter λ ; hence, these need to be appropriately determined. In this study, a combination of these parameters was determined by cross-validation (Stone, 1947) and Bayesian optimization (Močkus, 1975).

2.3 Search for the optimal placement using a genetic algorithm

A genetic algorithm (Holland, 1992) was used in this study for investigating optimal placement. Genetic algorithms search for approximate solutions of data, where multiple individuals whose solution candidates are expressed with genes are prepared, individuals with high fitness are preferentially selected, and solutions are searched for by repeating operations such as crossover and mutation. The problem targeted in this study includes an extremely large number of assessment points; furthermore, checking all combinations is extremely inefficient. Hence, we adopted an efficient genetic algorithm for the combination optimization problem.

Figure 2 shows an overview of the genetic algorithm. In this study, the point number was placed in the component of each individual, and optimization of those combinations was performed with a genetic algorithm. First, the number of individuals was determined, and a combination of points to be selected was randomly determined for the initial individuals. Next, the fitness was calculated for the generated individuals. Two individuals that are to be the parents of the next generation were then selected according to the obtained fitness. The parent selection method involves selecting individuals with high fitness as parents; low-fitness individuals are thus eliminated. The next generation of individuals is generated by randomly exchanging each component for the two selected parents. The location of exchange and the number of exchanges are randomly determined. This is repeated until the number of individuals in the next generation reaches the initially set number. In this study, we adopted an elite conservation strategy as a method to avoid deterioration of fitness during generational change, with settings such that some of the top individuals with high fitness could be passed on to the next generation as is. The final next-generation individuals were determined by mutating each component of each individual with a certain probability. In this process, the point number may be duplicated within one individual, and in such cases, the duplicated point is randomly re-selected. This process was repeated until the fitness converged, and an optimal point combination was determined.

3 Application to cases assuming an actual tsunami

The method described in the previous section was applied to a problem in which an actual tsunami was assumed. In this study, we conducted a series of numerical analyses that considered the uncertainty with the 2011 Off the Coast of Tohoku Earthquake as the target. We applied mode decomposition on these results to construct a surrogate model of the numerical analysis, and we implemented Monte Carlo simulations in order to investigate the optimal placement of facilities based on probability theory.

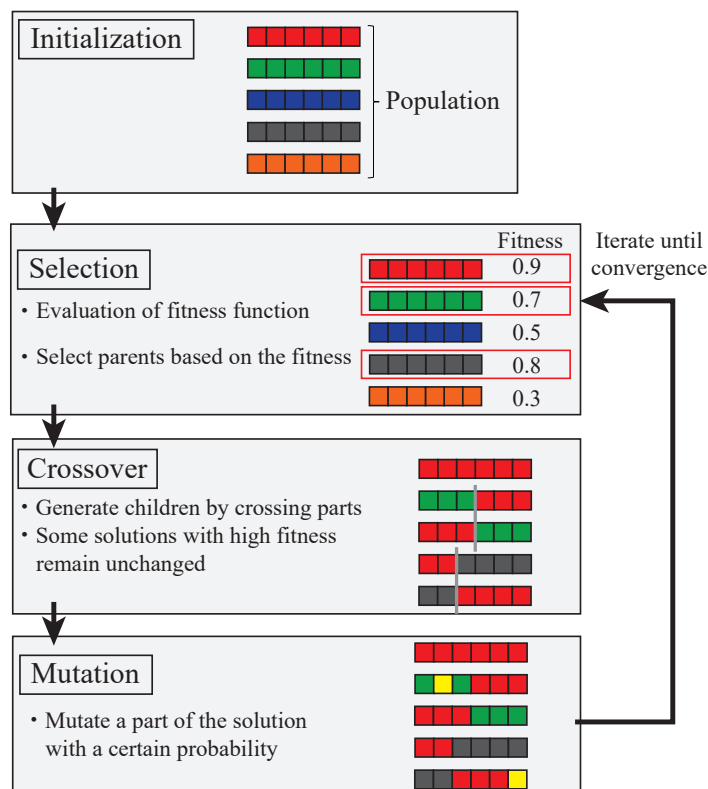


Figure 2. Flow of the genetic algorithm.

3.1 Tsunami simulation

200 We used the same numerical analysis results as those conducted in previous research (Tozato et al., 2022). The reader is referred to the study by (Tozato et al., 2022) for details regarding the computational conditions. The parameter values at the time of the Off the Coast of Tohoku Earthquake were set as mean values, with the slip varying between 0.7 and 1.4 times, and the rake varying between -20° to $+25^\circ$. The illustration of the fault parameters is shown in Fig. 3. Table 1 shows all analysis cases. In this study, the validity of the constructed surrogate model was verified by holding cases in which the rake was $\pm 10^\circ$ among
205 the 50 cases shown in Table 1; the remaining 40 cases were used to construct the surrogate model.

Figures 4 and 5 show the target area and snapshots of the analysis results of the inundation area for the mean case (S3R5), respectively. Figure 6 shows the results of comparison of the inundation depth with the actually observed inundation depth. The observed data were referenced from (The 2011 Tohoku Earthquake Tsunami Joint Survey Group, 2012), and the placement of the observation points from A to H is shown in Fig. 4. These results show that although there was some deviation between
210 the numerical analysis results and observed results at locations far away from the shore, the observation values were generally reproduced in the areas around the shore. The deviation between the numerical analysis results and the values observed in the

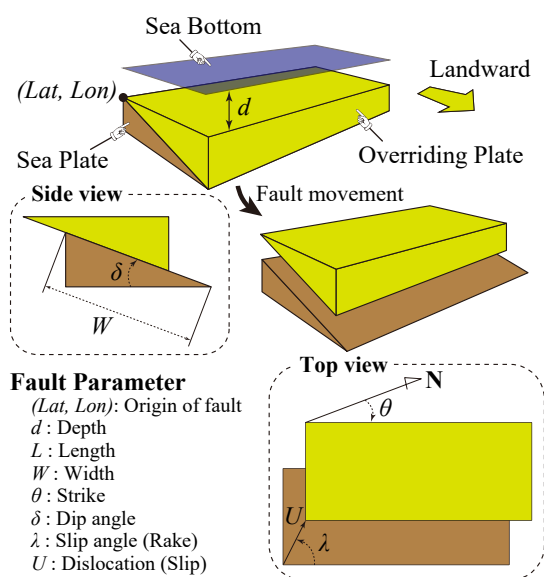


Figure 3. Illustration of the fault parameters. (adapted from Kotani et al. (2020)).

Table 1. Names of the calculation cases.

		Rake										
		[°]	-20	-15	-10	-5	0	+5	+10	+15	+20	+25
	[%]	Normalized value	0.753	0.815	0.877	0.938	1	1.062	1.123	1.185	1.247	1.309
Slip	70	0.7	S1R1	S1R2	S1R3	S1R4	S1R5	S1R6	S1R7	S1R8	S1R9	S1R10
	85	0.85	S2R1	S2R2	S2R3	S2R4	S2R5	S2R6	S2R7	S2R8	S2R9	S2R10
	100	1	S3R1	S3R2	S3R3	S3R4	S3R5	S3R6	S3R7	S3R8	S3R9	S3R10
	120	1.2	S4R1	S4R2	S4R3	S4R4	S4R5	S4R6	S4R7	S4R8	S4R9	S4R10
	140	1.4	S5R1	S5R2	S5R3	S5R4	S5R5	S5R6	S5R7	S5R8	S5R9	S5R10



locations far away from the shore was thought to be because the outflows of the buildings were not considered; hence, the waves did not reach the locations far away from the shore.



Figure 4. Boundary between 2D and 3D analyses areas. Points A to H are used to compare the inundation depths between the observational data and simulation results. (©Google Maps)

In this study, the physical values of the impact force acting on the buildings and the inundation depth were adopted as tsunami risk indices. The effects of the tsunami fluid force have been considered even in recent design criteria (American Society of Civil Engineers, 2017; Nakano, 2017); therefore, we considered the fluid force acting on buildings as an additional risk index to the inundation depth. A 3D simulation was conducted to construct a surrogate model of the tsunami fluid force; however, the tsunami fluid force is strongly influenced by the direction that the building is facing, and it is difficult to assess the fluid force for each point. Therefore, the tsunami fluid force was assessed with a 2D grid size of approximately 10 m in this study. An image of a mesh for evaluating the tsunami force is shown in Fig. 7. The target area was $2,145 \times 2,600$ m; hence, the number of assessment points in the POD was $n = 214 \times 260 = 55,640$.

3.2 Construction of a surrogate model with POD

POD was applied on the numerical analysis results to construct a surrogate model. When applying the POD, the data at each point were normalized in advance to a mean value of 0 and standard deviation of 1. Figure 8 shows the spatial modes extracted by the POD from the first mode to the third mode. The values shown in the figure are values of the eigenvectors, and these were adjusted so that the maximum absolute value of the components in the eigenvectors was 1. The characteristics of the spatial distribution could be read for each physical quantity from the spatial modes. A comparison of the spatial modes of the maximum impact force and maximum inundation depth confirmed that the three modes shown here have similar characteristics.

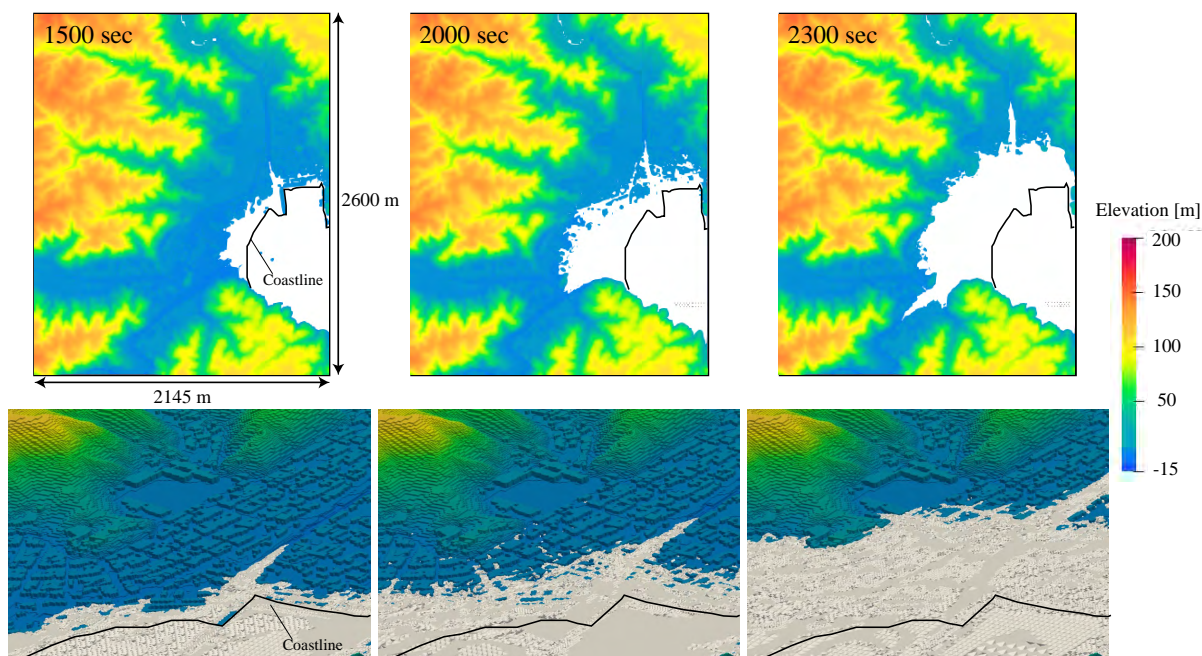


Figure 5. Snapshots of the tsunami runup obtained through 3D analysis.

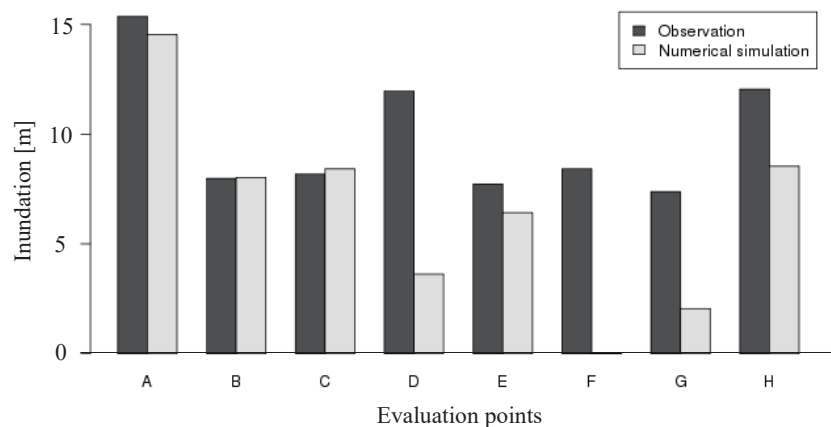


Figure 6. Comparison of the inundation between observational data and numerical simulation. (Observation data are provided by field survey results (The 2011 Tohoku Earthquake Tsunami Joint Survey Group, 2012)).

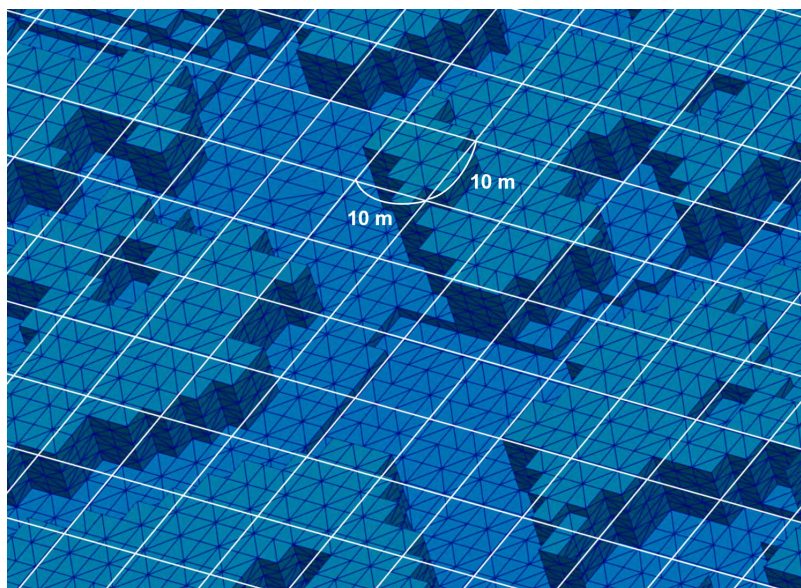


Figure 7. Image of a mesh for evaluating tsunami force.

For example, in the first mode, the sign was the same overall, and the value on the coast side was large; thus, the mode showed
230 an overall tendency where the coast side was the most affected by the tsunami, with the effect becoming smaller moving away
from the coast. In the second mode, a tendency could be seen where the maximum impact force and maximum inundation
depth were opposite at the east and west sides. In the third mode, a tendency could be seen where the maximum impact force
and maximum inundation depth were opposite at the north and south sides. These modes were thought to be related to the
inflow direction of the tsunami. Furthermore, higher-dimension modes included the characteristics of local sections. Figure 9
235 shows the contribution rates of the modes. The contribution rate of the first mode was extremely high for both the maximum
impact force and maximum inundation depth.

Next, the coefficients of each mode were expressed as a function of the uncertainty parameters. As previously mentioned,
RBF interpolation shown in Eq. (14) was used, and the regularization shown in Eq. (17) was introduced in the calculation to
obtain the weight. The accuracy of the surrogate model changed according to the RBF smoothness parameter and regularization
240 parameter; thus, it is important to appropriately determine these. In this study, these parameters were determined using cross-
validation.

The learning and verification cases used for cross-validation were obtained by taking a total of 40 cases used in the con-
struction of the surrogate model, removing four cases that correspond to the corners of the parameter space (S1R1, S1R10,
S5R1, S5R10), and dividing the remaining 36 cases between learning and verification cases for cross-validation. The corner
245 data were not used for the verification cases because these data were extrapolated. In this example, the number of divisions
between the learning and verification cases was set to 12. In other words, the policy was to construct a model with 37 cases

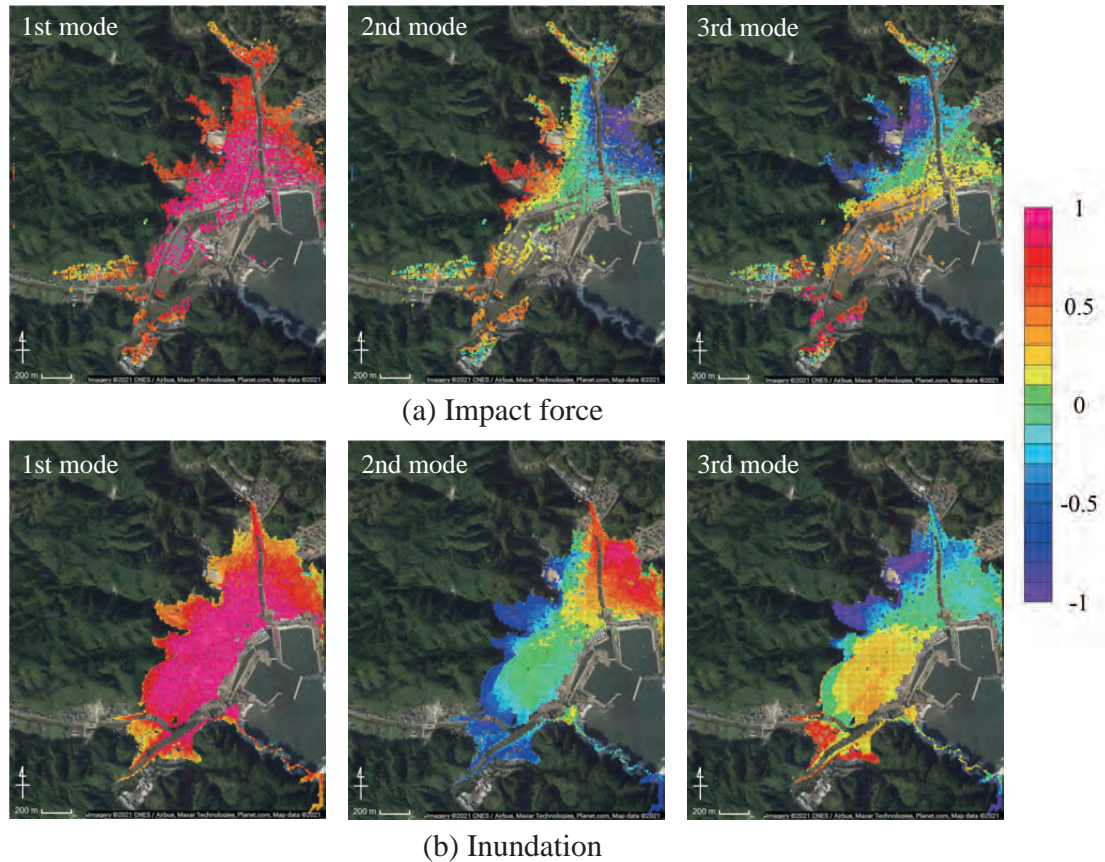


Figure 8. Spatial modes for each risk index extracted by POD. (left: 1st mode, middle: 2nd mode, right: 3rd mode) (©Google Maps)

for a single verification and conduct verification using three cases. Furthermore, the cross-validation error was calculated by comparing the reconstructed results using the spatial mode and taking the ratio of the mean absolute error to the mean value as shown in the following equation.

$$e_r = \frac{\frac{1}{nN} \sum_{i=1}^n \sum_{j=1}^N |x_{ij} - \hat{x}_{ij}|}{\frac{1}{nN} \sum_{i=1}^n \sum_{j=1}^N x_{ij}} \quad (18)$$

Here, n is the number of assessed values, N is the number of scenarios, and x_{ij} is the numerical analysis result for scenario i and point j . Furthermore, \hat{x}_{ij} is the value for scenario i and point j when reconstructed with the surrogate model, and e_r is the error when the number of modes is r .

Figure 10 shows the results of calculations of the maximum impact force and maximum inundation depth for the cross-validation error in each mode. Cases in which no regularization term is present (Eq. (15)) are also shown. Bayesian optimization was used for the search in the parameter space, the number of searches was set to 80, and the upper confidence bound (UCB) strategy was used for the acquisition function. The state of error change confirmed that the accuracy of the surrogate model

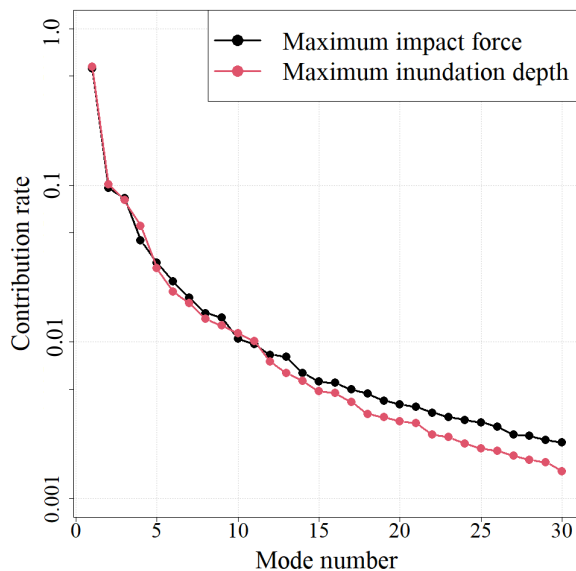


Figure 9. Contribution rates for each risk index.

was improved because the error value was reduced by introducing the regularization term. By introducing the regularization term, a robust surrogate model can be constructed.

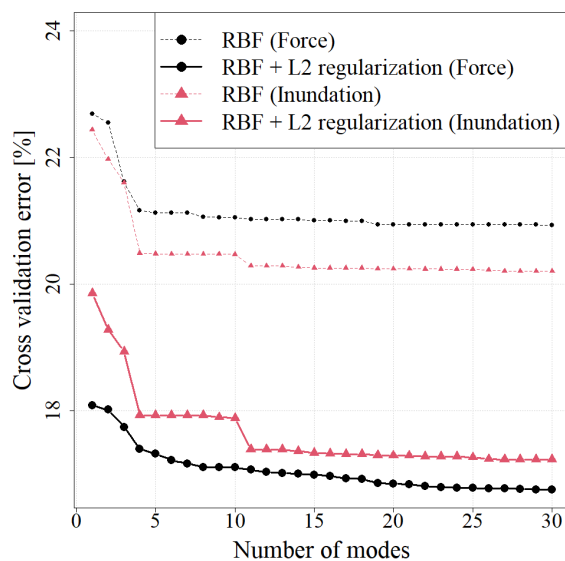


Figure 10. Cross-validation error for each mode.



260 Finally, the validity of the surrogate model was verified by comparing the results obtained from the numerical simulations
for the scenarios that were not used for the constructed surrogate model with the results of the constructed surrogate model.
Figure 11 shows a comparison of the numerical simulation results and the results obtained from the surrogate model for the
S3R3 scenario. Regarding the number of modes used in the surrogate model, the maximum impact force was set to 8 and
the maximum inundation depth was set to 11. The validity of the surrogate model can be confirmed because the figure shows
265 that the spatial distribution is generally reproduced. Furthermore, Fig. 12 shows the results of assessing the errors of the 10
scenarios that were held for verification. The error was calculated using Eq. (18). The error values as well that the numerical
analysis results were generally reproduced.

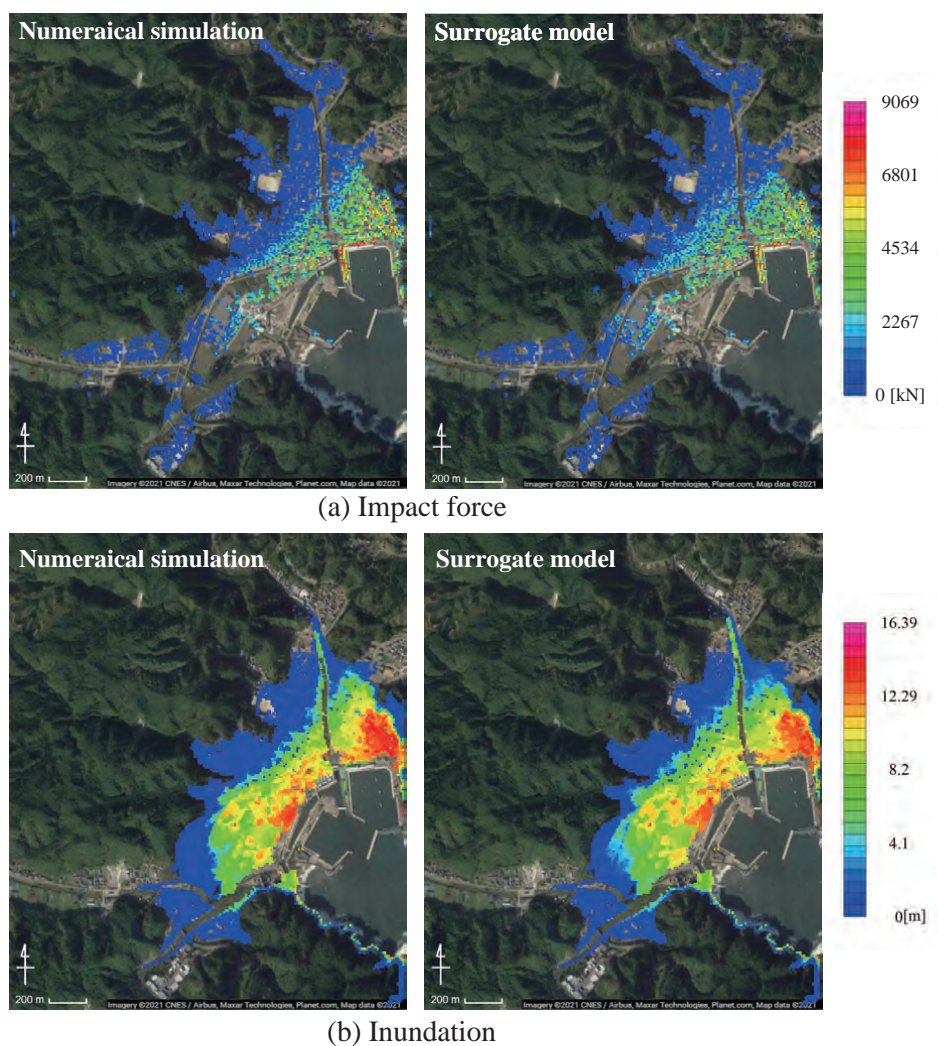


Figure 11. Comparison between results of numerical simulation and the surrogate model. (Scenario: S3R3) (© Google Maps)

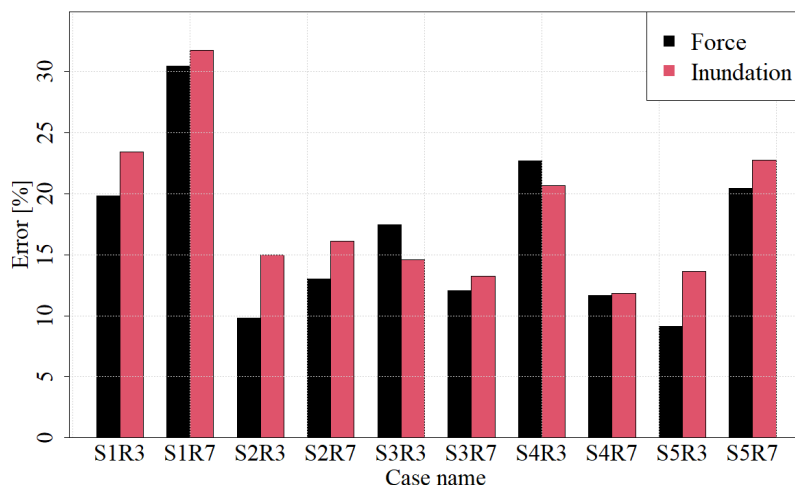


Figure 12. Errors between the numerical simulation and surrogate model for each validation scenario.

3.3 Monte Carlo simulation

We conducted probabilistic tsunami risk assessments using the surrogate model shown in the previous section. The surrogate model enables the computation of a spatial distribution of risk indices at low computational cost; hence, many trials can be secured at a relatively low computational cost, and a risk assessment that efficiently utilizes the advanced numerical simulation results can be conducted.

In this study, we conducted a probabilistic assessment of the tsunami risk by applying Monte Carlo simulations. The uncertainty of the changes in the input parameters must be quantitatively assessed in a probabilistic manner for Monte Carlo simulations. We assumed that the slip and rake followed a normal distribution, and the probability distribution parameters were set as shown in Table 2. The rationale for setting the values in this table is as follows. For the mean values, as mentioned in the previous section, normalized values were used as the input parameters, so these were set as 1.0. Furthermore, for the standard deviation of the slip, a value of 0.1 was used, which indicates a standard deviation value that is 10% of the mean value. For a normal distribution, the spread of approximately three times the given standard deviation is present; thus, the value of three times the standard deviation was set as this value so that the range of Table 1 in the previous section was covered. Furthermore, for the standard deviation of the rake, Japan Society of Civil Engineering (2011) conducted probabilistic assessments where the rake was varied by $\pm 10^\circ$; therefore, in this study as well, we considered this degree of variation, and a value of 0.04 was used, which was considered to result in a variation of approximately three times the standard deviation.

Monte Carlo simulations were conducted using the input parameters listed in Table 2 and the surrogate model. Specifically, the uncertainty information of each input parameter was used to randomly generate a combination of the slip and rake; this value was assigned to the function of the surrogate model coefficient component, and a value that was multiplied by the mode was added according to the number of modes to calculate the spatial distribution of the risk index. This was repeated for the



Table 2. Information on the variation of uncertainty parameters.

Parameter	Mean	Standard deviation
Slip	1.0	0.1
Rake	1.0	0.04

number of trials, which was set to 10,000 in this study, and the probability density distributions of the maximum impact force and maximum inundation depth at each point were calculated.

290 Maps of exceedance probability are obtained from the results of Monte Carlo simulations. The exceedance probability at each evaluation point is calculated assuming the failure that can be defined by the criteria of risk indices. Based on the previous studies (Suppasri et al., 2013, 2019), we defined the criteria as 176 kN for the maximum impact force and 3 m for the maximum inundation depth. The obtained exceedance probability maps for both risk indices are shown in Fig. 13. In both maps, there is a tendency that high exceedance probabilities arise near the coast and low exceedance probabilities occur farther away from the coast. On the other hand, there are some differences between the maps locally. For example, the exceedance probability of the maximum impact force tends to be high in the areas where there are many buildings. Since the computational cost of surrogate models are quiet low, such probabilistic maps can be easily obtained.

295

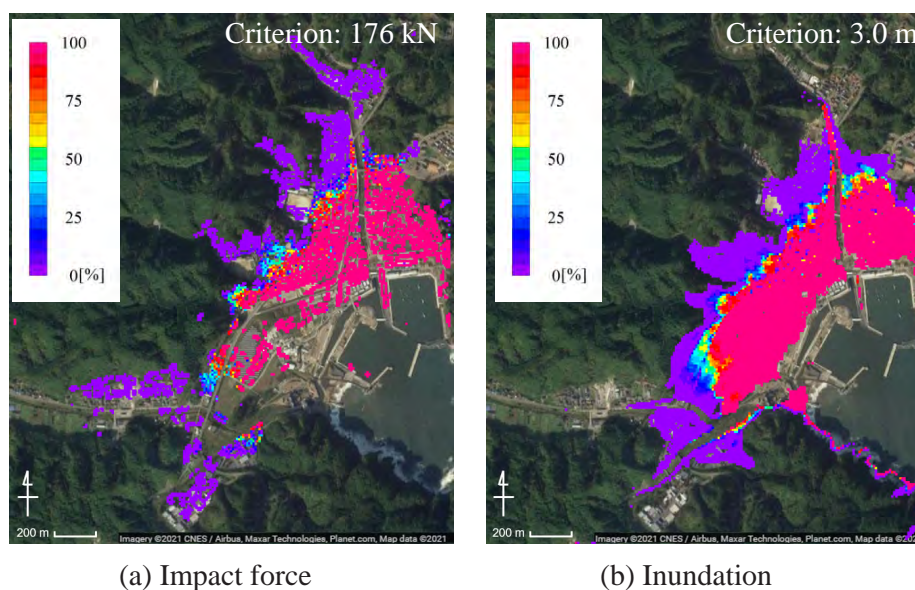


Figure 13. Spatial distribution for the exceedance probability. (©Google Maps)



3.4 Optimal placement of system using genetic algorithms

The results of Monte Carlo simulation are used to investigate an optimal placement of the system. The optimal placement is examined based on the concepts of both parallel and series systems, and the results are compared. In the case of a parallel system, the system failure is considered to occur when all of its components have failed. On the other hand, regarding a series system, the system is considered to be have failed when any one of its components is destroyed.

In this study, the optimization problem is defined to select the components of the system from the evaluation points used in the construction of the surrogate model. The areas that have 25% or higher exceedance probabilities for each failure criteria are set as the target areas. The reason why the components of the system were selected only in these high risk areas is that a point with an exceedance probability of 0% should be always selected if there are such points in the target area, and this does not result in a optimal problem. This condition is not so realistic, but we employed it as a calculation condition to clearly represent the performance of the proposed method.

For the settings of the genetic algorithm, the number of individuals was set to 200, and the mutation probability was set to 10% for each component of each individual. Furthermore, we adopted an elite conservation strategy; in each generation, when there is no other individual that simultaneously improves both objective functions, the individuals of the current generation are passed on to the next generation as is. Moreover, the solutions near the optimal solution are likely to be selected for the crossover. In this study, the solution convergence was set as that when the solution individuals do not change over 2,000 steps. We investigated cases in which the number of components is 4 for each failure criterion and each system. Since the solution may depend on on the initial conditions, we hence conducted three trials under the same conditions for each case.

The results of optimal placements based on the concepts of the parallel and series systems for each risk index are shown in Fig. 14. In these figures, the results are also compared with the placements determined based on a simple strategy, in which the components of the system are selected in order of lower exceedance probability. White points shown in Fig. 14 indicate the components of the system selected by the genetic algorithm, and black points show the components selected in order of lower exceedance probability. System failure probabilities for each placement are shown in Table 3. The system failure probabilities are expressed as the probability of failure of all components for the parallel system and the probability of failure of one or more components for the series system.

Table 3. System failure probability for each risk index and each system.

	Impact force		Inundation	
	Parallel	Series	Parallel	Series
Minimum failure probability [%]	20.94	29.62	22.50	28.03
Genetic algorithm [%]	19.40	28.09	0.10	25.50

According to the results shown in Fig. 14, it is found that the selected components are placed away from the coast line. This tendency comes from the fact that low failure probability points are generally located away from the coastal region. Different

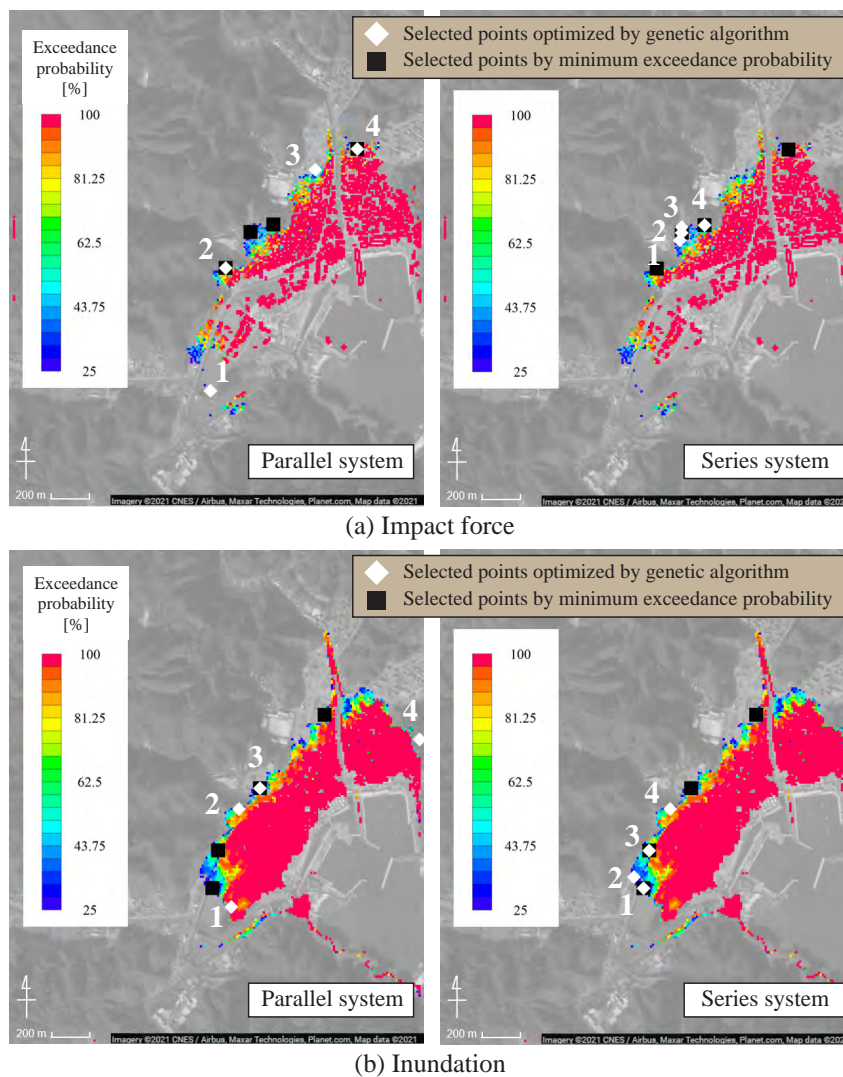


Figure 14. Optimal placements obtained from the genetic algorithm for each risk index. (©Google Maps) Selected points by minimum exceedance probability shows the results of placements determined in order of decreasing exceedance probability at each evaluation point. Only search areas are colored in this figure.



325 placements were obtained for the maximum impact force and inundation depth. Comparing the parallel and series systems, it
can be seen that the components are selected by concentrating on similar locations in the series system, while the components
are selected by spatially dispersing them in the parallel system. Regarding the series system, where all failures of one or more
components would result in the destruction of the system, the components are concentrated in such an arrangement that the
probability of exceedance is small. On the contrary, one or more of the components need only be safe in a parallel system. That
330 is why the components are spatially distributed.

Through the comparison of the obtained optimal placements for all systems, it can be seen that some common locations
were selected for some components, but different locations were also selected for others. Although different placements were
obtained, the risk for both parallel and series systems as shown in Table 3.

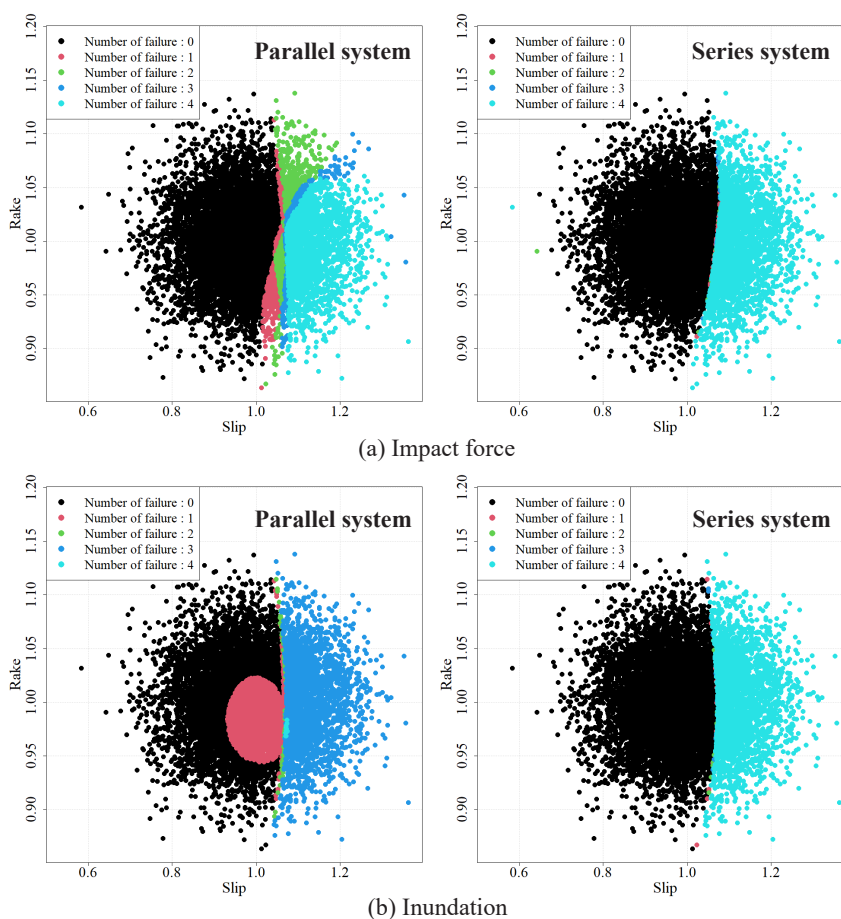


Figure 15. The scatter plot of the uncertainty parameters colored by the number of failure points for each placement.

A detailed analysis of the placements selected for each system was performed. Figure 15 shows the scatter plots of the
335 uncertainty parameters, slip and rake, considered in the Monte Carlo simulation, and the number of failure components is



colored. The placement for the parallel system optimizes around a smaller light blue area and the placement for the series system optimizes around a larger black area. According to Fig. 15, the slip mainly contributes to the failure of each point and the system for all placements because no failure occurs in smaller-slip cases and the failure occurs in the high-slip case. The rake contributes to the parallel system placement because the number of failure points changes in the same slip values for the parallel system.

In the series system, the scenarios are separated into two situations; all safe and all destroyed. In contrast, the parallel system shows a more complex placement pattern. Figure 16 shows a colored scenario in the uncertainty parameter space. As can be seen in Fig. 16, regarding the maximum impact force, it can be seen that the components are selected such a way that they are not destroyed depending on the value of the rake. On the other hand, in the case of the inundation depth, it can be confirmed that component 4 has unique tendency compared to the other components. As we can understand from this numerical example, the optimal placement is efficiently discussed by the method proposed in this study.

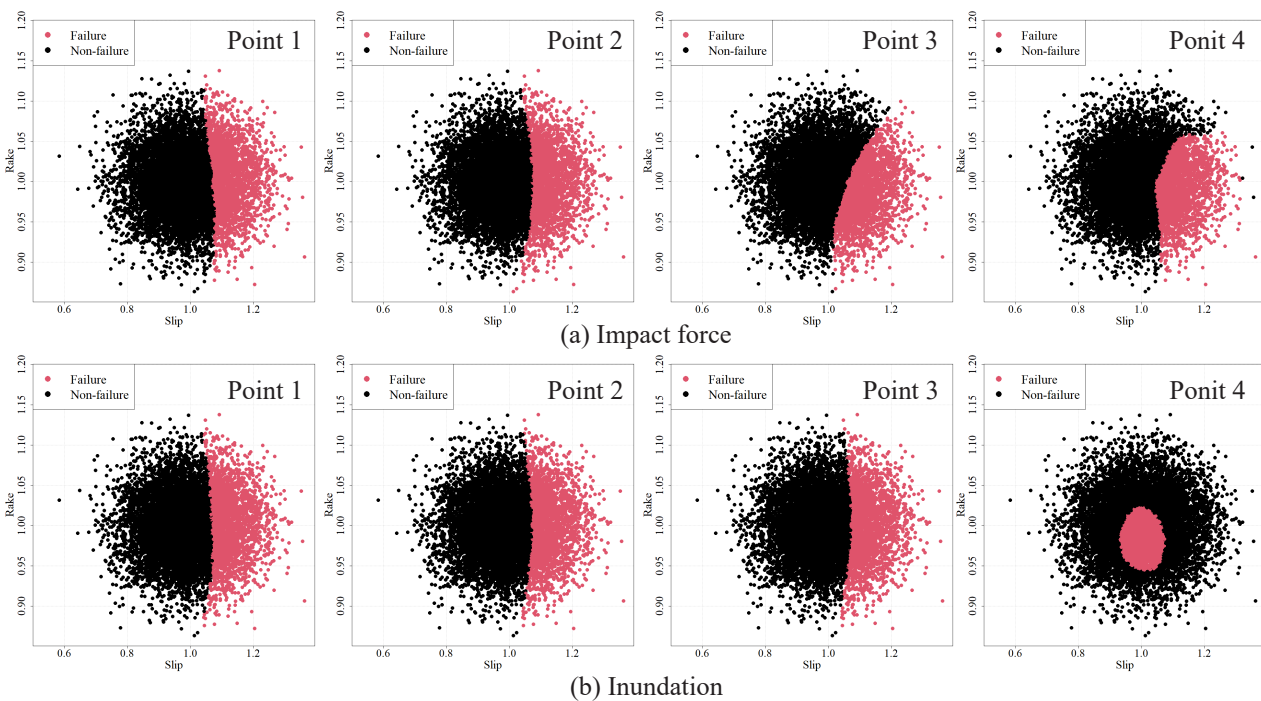


Figure 16. The scatter plot of the uncertainty parameters colored by failure or non-failure for each placement in inundation case.

Using the results of the Monte Carlo simulation using the surrogate models, the optimal system placements can be probabilistically investigated based on information from the advanced numerical simulation. This method could be used to solve the problem of optimal placement of facilities such as relief bases, shelters, and infrastructure facilities during disasters.



350 4 Conclusions

In this study, we used advanced 3D simulation results to construct a surrogate model, and we used this model to propose a method that enabled the efficient investigation of the optimal placement of facilities based on probability theory. We constructed a surrogate model by applying POD to 3D numerical simulation results of tsunamis, and Monte Carlo simulations that used this surrogate model were conducted to show that it was possible to assess the probability density distribution of risk indices at all 355 points within the target area and the spatial distribution of exceedance probability with a low computational cost. Furthermore, we show that applying the genetic algorithm to Monte Carlo simulations enabled the search for the optimal placement of parallel and series systems, which minimized failure in a probabilistic manner. In this way, the proposed method enabled the investigation of the optimal placement of facilities in a probabilistic manner by efficiently utilizing the information obtained from advanced numerical simulations.

360 The uncertainty parameters in this study were limited to two when conducting assessments; however, there are more uncertainties than this in actual phenomena. Thus, it is important to conduct a probabilistic risk assessment that considers this fact. Furthermore, the extent to which each uncertainty parameter will fluctuate must be assessed in advance to determine cases in which numerical simulations or Monte Carlo simulations are to be conducted. The surrogate model that was constructed with the proposed method is capable of assessments with sufficient accuracy for interpolation (within the range of uncertainty 365 parameters for which numerical simulations were conducted); however, the accuracy often decreases for cases of extrapolation (outside the range of uncertainty parameters for which the numerical simulations were conducted); thus, an assessment of uncertainty fluctuation is important. In addition, since the accuracy of the surrogate model changes according to the number of spatial modes, it's necessary to establish a way of properly determining the number of modes in future works. It is also noted that we calculated the exceedance probability with the destruction criterion as a constant when investigating the exceedance 370 probability and optimal placement; however, the destruction criteria vary according to the building material. Thus, the use of this information would enable a more advanced probabilistic risk assessment and optimal placement of facilities.

Appendix A: Verification of the validity of the numerical analysis method

In this study, we conducted a comparison with the experimental results of the study by Winter et al. (2020) and verified the validity of the 3D analysis method adopted in this study. In the study by Winter et al. (2020), experiments were conducted on the 375 fluid force acting on the structure while changing the structural placement; in this study, we conducted a comparison between the experiment results under the conditions shown in Fig. A1 among the aforementioned changes in structure placement with the analysis results. Details of the experiment are as shown in the study by Winter et al. (2020), and a comparison was performed with the numerical analysis results regarding the temporal changes in the water level on the front side of the structure and the fluid force acting on the structure. Fig. A2 shows the comparison results for each case. As shown in the figure, the validity of 380 the adopted numerical analysis could be confirmed because the fluid force and water depth tendencies were generally captured. Furthermore, Fig. A3 shows a snapshot of the simulation results.

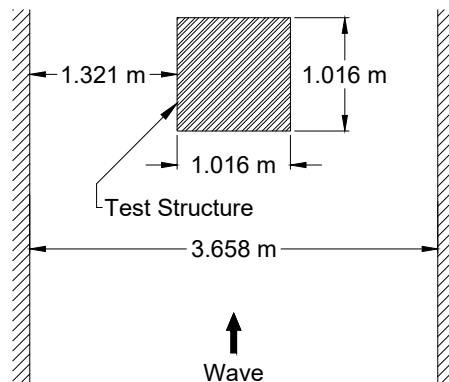


Figure A1. Configuration of the test structure.

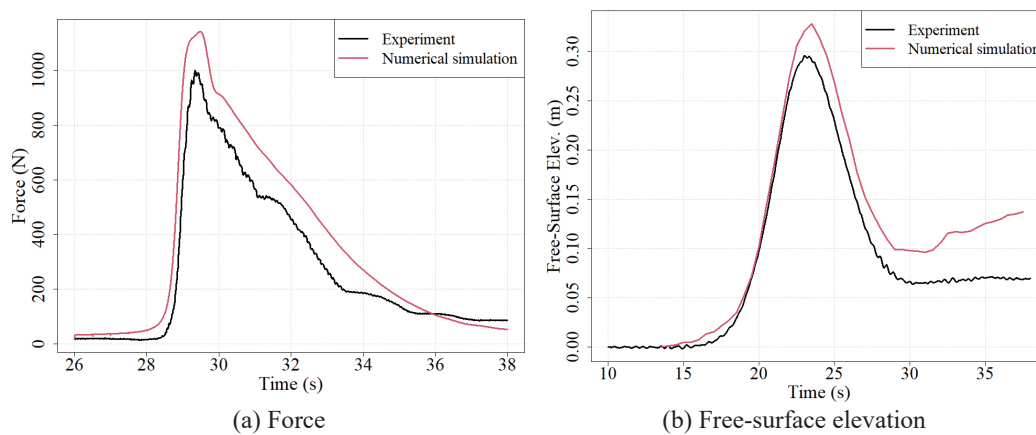


Figure A2. Comparison between the experimental results and numerical simulation results. ((a) Force, (b) Free-surface elevation)

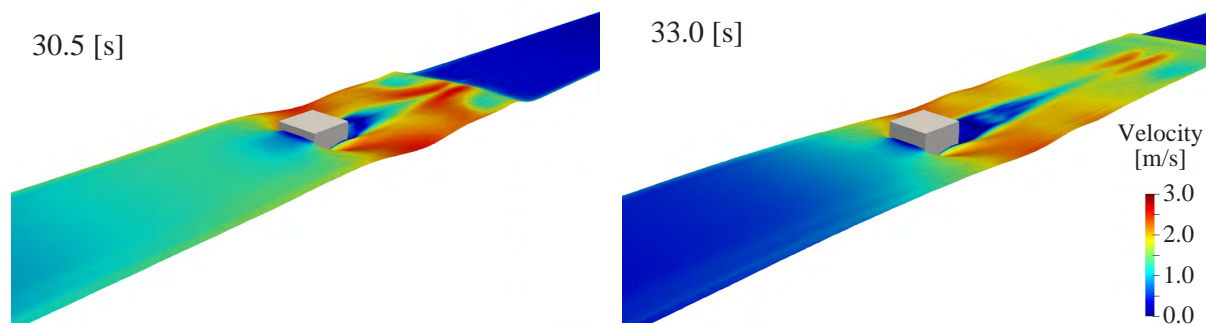


Figure A3. Snapshot of the numerical simulation result.



Code and data availability. Source code and details of the tsunami simulation were sourced from Kotani et al. (2020). Outputs of the simulations are available the Zenodo open-access repository at <https://doi.org/10.5281/zenodo.6394294> (Tozato , 2022).

Author contributions. KTo contributed to methodology, analyses, and preparing the original manuscript. SM contributed to the conceptualization and methodology, and prepared the manuscript. ST contributed to the numerical simulations. YO and AS contributed to the methodology and conceptualization. MM contributed to the investigation and reviewing the manuscript. KTe contributed to the supervision and reviewing the manuscript.

Competing interests. The authors declare that they have no conflict of interest.



References

- 390 Annaka, T., Satake, K., Sakakiyama, T., Yanagisawa, K., Shuto, N.: Logic-tree approach for probabilistic tsunami hazard analysis and its applications to the Japanese coasts. *Pure Appl. Geophys.* 164(2), 577–592, <https://doi.org/10.1007/s00024-006-0174-3>, 2007.
- Bamer, F., Bucher, C.: Application of the proper orthogonal decomposition for linear and nonlinear structures under transient excitations. *Acta Mechanica* 223(12), 2549–2563, <https://doi.org/10.1007/s00707-012-0726-9>, 2012.
- Buhmann, M.D.: Multivariate cardinal interpolation with radial-basis functions. *Constr. Approxim.* 6(3), 225–255, <https://doi.org/10.1007/BF01890410>, 1990.
- 395 Cavdur, F., Kose-Kucuk, M., Sebatli, A.: Allocation of temporary disaster-response facilities for relief-supplies distribution: A stochastic optimization approach for after disaster uncertainty, *Natural Hazards Review*, 22(1), 05020013, [https://doi.org/10.1061/\(ASCE\)NH.1527-6996.0000416](https://doi.org/10.1061/(ASCE)NH.1527-6996.0000416), 2020.
- Cavdur, F., Sebatli-Saglam, A., Kose-Kucuk, M.: A spreadsheet-based decision support tool for temporary-disaster-response facilities allocation. *Saf. Sci.* 124, 104581, <https://doi.org/10.1016/j.ssci.2019.104581>, 2020.
- 400 Cornell, C. A.: Engineering seismic risk analysis. *Bull. Seismol. Soc. Am.* 58(5), 1583–1606, <https://doi.org/10.1785/BSSA0580051583>, 1968.
- Doerner, K.F., Gutjahr, W.J., Nolz, P.C.: Multi-criteria location planning for public facilities in tsunami-prone coastal areas. *OR Spectrum* 31, 651–678, <https://doi.org/10.1007/s00291-008-0126-7>, 2008.
- 405 Fukutani, Y., Moriguchi, S., Terada, K., Otake, Y.: Time-dependent probabilistic tsunami inundation assessment using mode decomposition to assess uncertainty for an earthquake scenario. *Journal of Geophysical Research: Oceans*, 126, e2021JC017250, <https://doi.org/10.1029/2021JC017250>, 2021.
- Fukutani, Y., Suppasri, A., Imamura, F.: Stochastic analysis and uncertainty assessment of tsunami wave height using a random source parameter model that targets a Tohoku-type earthquake fault. *Stoch. Environ. Res. Risk Assess* 29(7), 1763–1779, <https://doi.org/10.1007/s00477-014-0966-4>, 2015.
- 410 Geist, E.L., Parsons, T.: Probabilistic analysis of tsunami hazards*. *Nat. Hazards* 37(3), 277–314, <https://doi.org/10.1007/s11069-005-4646-z>, 2006.
- Gomez, C., Baker, J.W.: An optimization-based decision support framework for coupled pre- and post-earthquake infrastructure risk management. *Struct. Saf.* 77, 1–9, <https://doi.org/10.1016/j.strusafe.2018.10.002>, 2019.
- 415 Goto, C., Ogawa, Y., Shuto, N., Imamura, F.: Numerical method of tsunami simulation with the leap-frog scheme. *IUGG/IOC TIME Project, IOC Manual and Guides*, 35, 1–126, 1997.
- Ha, D.M., Tkalich, P., Chan, E.S.: Tsunami forecasting using proper orthogonal decomposition method. *J. Geophys. Res. Oceans* 113(C6), <https://doi.org/10.1029/2007JC004583>, 2008.
- Hoerl, A.E., Kennard, R.W.: Ridge regression: Biased estimation for nonorthogonal problems. *Technometrics* 12(1), 55–67, <https://doi.org/10.1080/00401706.1970.10488634>, 1970.
- 420 Holland, J.H.: *Adaptation in Natural and Artificial Systems*, second edition, University of Michigan Press, Ann Arbor, MI, 1992, 1992.
- Hotelling, H.: Analysis of a complex of statistical variables into principal components. *J. Educ. Psychol.* 25(6), 417–441, <https://psycnet.apa.org/doi/10.1037/h0071325>, 1933.
- Imamura, F.: Review of tsunami simulation with a finite difference method, in *Long-Wave Runup Models*, edited by H. Yeh, P. Liu, and C. Synolakis, World Scientific Publishing, Hackensack, N. J., 25–42, <https://doi.org/10.1142/9789814530330>, 1995.
- 425



- Ishikawa, Y., Kameda, H.: Hazard-consistent magnitude and distance for extended seismic risk analysis. Proceedings of the 9th World Conference on Earthquake Engineering. Tokyo-Kyoto, 89–94, 1988.
- Japan Society of Civil Engineering. The method of probabilistic tsunami hazard analysis (in Japanese), 2011.
- Jolliffe, I.T., Cadima, J.: Principal component analysis: a review and recent developments. *Philos. Trans. R. Soc. A Math. Phys. Eng. Sci.* 374(2065), 20150202, <https://doi.org/10.1098/rsta.2015.0202>, 2016.
- 430 Karhunen, K.: Uber lineare methoden in der wahrscheinlichkeitsrechnung. *Annals of Academic Science Fennicae, Series A1 Mathematics and Physics*, 37, 3–79, 1947.
- Kerschen, G., Golinval, J.C., Vakakis, A.F., Bergman, L.A.: The method of proper orthogonal decomposition for dynamical characterization and order reduction of mechanical systems: An overview. *Nonlinear Dyn.* 41(1), 147–169, <https://doi.org/10.1007/s11071-005-2803-2>,
435 2005.
- Kosambi, D.D.: Statistics in function space. *J. Indian Math. Soc.* 7, 76–88, 1943.
- Kotani, T., Tozato, K., Takase, S., Moriguchi, S., Terada, K., Fukutani, Y., Otake, Y., Nojima, K., Sakuraba, M., Choe, Y.: Probabilistic tsunami hazard assessment with simulation-based response surfaces. *Coast. Eng.* 160, 103719, <https://doi.org/10.1016/j.coastaleng.2020.103719>, 2020.
- 440 LeVeque, R.J., Waagan, K., Gonz´alez, F.I., Rim, D., Lin, G.: Generating random earthquake events for probabilistic tsunami hazard assessment. *Pure Appl. Geophys.* 173(12), 3671–3692, <https://doi.org/10.1007/s00024-016-1357-1>, 2016.
- Maharjan, R., Hanaoka, S.: A credibility-based multi-objective temporary logistics hub location- allocation model for relief supply and distribution under uncertainty. *Socio-Econ. Plan. Sci.* 70, 100727, <https://doi.org/10.1016/j.seps.2019.07.003>, 2020.
- McGuire, R.K.: Seismic design spectra and mapping procedures using hazard analysis based directly on oscillator response. *Earthq. Eng. Struct. Dyn.* 5(3), 211–234, <https://doi.org/10.1002/eqe.4290050302>, 1977.
- 445 Melgar, D., LeVeque, R.J., Dreger, D.S., Allen, R.M.: Kinematic rupture scenarios and synthetic displacement data: An example application to the Cascadia Subduction Zone. *J. Geophys. Res. Solid Earth* 121(9), 6658–6674, <https://doi.org/10.1002/2016JB013314>, 2016.
- Miller, M., Baker, J.: Ground-motion intensity and damage map selection for probabilistic infrastructure network risk assessment using optimization. *Earthq. Eng. Struct. Dyn.* 44, 1139–1156, <https://doi.org/10.1002/eqe.2506>, 2015.
- 450 Minimum Design Loads and Associated Criteria for Buildings and Other Structures. American Society of Civil Engineers, ASCE/sei 7-16 edition, 2017.
- Mitsoudis, D.A., Flouri, E.T., Chryssoulakis, N., Kamarianakis, Y., Okal, E.A., Synolakis, C.E.: Tsunami hazard in the Southeast Aegean Sea. *Coast. Eng.* 60, 136–148, <https://doi.org/10.1016/j.coastaleng.2011.09.004>, 2012.
- Moćkus, J.: On bayesian methods for seeking the extremum. Springer, Berlin, Heidelberg, https://doi.org/10.1007/3-540-07165-2_55, 1975.
- 455 Mohamadi, A., Yaghoubi, S.: A bi-objective stochastic model for emergency medical services network design with backup services for disasters under disruptions: An earthquake case study. *Int. J. Disaster Risk Reduc.* 23, 204–217, <https://doi.org/10.1016/j.ijdr.2017.05.003>, 2017.
- Mori, N., Goda, K., Cox, D.: Recent process in probabilistic tsunami hazard analysis (ptha) for mega thrust subduction earthquakes. The 2011 Japan Earthquake and Tsunami: Reconstruction and Restoration, pp. 469–485, https://doi.org/10.1007/978-3-319-58691-5_27, 2017.
- 460 Nakano, Y.: Structural design requirements for tsunami evacuation buildings in Japan. ACI Symposium Publication, 313, 2017.
- Nojima, N., Kuse, M., Duc, L.Q.: Mode decomposition and simulation of strong ground motion distribution using singular value decomposition. *JAEE* 18(2), 95–114, https://doi.org/10.5610/jaee.18.2_95, 2018.



- Park, H., Cox, D.T.: Probabilistic assessment of near-field tsunami hazards: Inundation depth, velocity, momentum flux, arrival time, and duration applied to seaside, Oregon. *Coast. Eng.* 117, 79–96, <https://doi.org/10.1016/j.coastaleng.2016.07.011>, 2016.
- 465 Park, S., van de Lindt, J.W., Gupta, R., Cox, D., 2021. Method to determine the locations of tsunami vertical evacuation shelters. *Nat. Hazards* 63, 891–908, <https://doi.org/10.1007/s11069-012-0196-3>, 2012.
- Pearson K.: F.R.S.: LIII. on lines and planes of closest fit to systems of points in space. *The London, Edinburgh, and Dublin Philosophical Magazine and Journal of Science*, 2(11), 559–572, <https://doi.org/10.1080/14786440109462720>, 1901.
- Power, W., Downes, G., Stirling, M.: Estimation of tsunami hazard in new Zealand due to south American earthquakes. *Pure Appl. Geophys.* 164(2), 547–564, https://doi.org/10.1007/978-3-7643-8364-0_15, 2007.
- 470 Qin, X., Motley, M.R., Marafi, N.A.: Three-dimensional modeling of tsunami forces on coastal communities. *Coast. Eng.* 140, 43–59, <https://doi.org/10.1016/j.coastaleng.2018.06.008>, 2018.
- Rawls, C.G., Turnquist, M.A.: Pre-positioning of emergency supplies for disaster response. *Transp. Res. B Methodol.* 44, 521–534, <https://doi.org/10.1016/j.trb.2009.08.003>, 2010.
- 475 Stone, M.: Cross-validators choice and assessment of statistical predictions. *Journal of the Royal Statistical Society. Series B (Methodological)*, 36(2), 111–147, <https://doi.org/10.1111/j.2517-6161.1974.tb00994.x>, 1947.
- Suppasri, A., Mas, E., Charvet, I., Gunasekera, R., Imai, K., Fukutani, Y., Abe, Y., Imamura, F.: Building damage characteristics based on surveyed data and fragility curves of the 2011 great east japan tsunami. *Nat. Hazards* 66, 319–341, <https://doi.org/10.1007/s11069-012-0487-8>, 2013.
- 480 Suppasri, A., Pakoksung, K., Charvet, I., Chua, C.T., Takahashi, N., Ornthammarath, T., Latcharote, P., Leelawat, N., Imamura, F.: Load-resistance analysis: An alternative approach to tsunami damage assessment applied to the 2011 great east Japan tsunami. *Nat. Hazards Earth Syst. Sci.* 19, 1807–1822, <https://doi.org/10.5194/nhess-19-1807-2019>, 2019.
- Takase, S., Moriguchi, S., Terada, K., Kato, J., Kyoya, T., Kashiya, K., Kotani, T.: 2D-3D hybrid stabilized finite element method for tsunami runup simulations. *Comput. Mech.* 58(3), 411–422, <https://doi.org/10.1007/s00466-016-1300-4>, 2016.
- 485 The 2011 Tohoku Earthquake Tsunami Joint Survey Group. Field survey results, official survey data, , <http://www.coastal.jp/tsunami2011/index.php?Field%20survey%20results> (last access: 21 March 2022), 2012.
- Thio, H.K., Somerville, P., Ichinose, G.: Probabilistic analysis of strong ground motion and tsunami hazards in Southeast Asia. *J. Earthq. Tsunami* 1(2), 119–137, <https://doi.org/10.1142/S1793431107000080>, 2007.
- Tozato, K., Takase, S., Moriguchi, S., Terada, K., Otake, Y., Fukutani, Y., Nojima, K., Sakuraba, M., Yokosu, H.: Rapid tsunami force prediction by mode-decomposition-based surrogate modeling. *Nat. Hazards Earth Syst. Sci. Disc.* 22, 1267–1285, <https://doi.org/10.5194/nhess-22-1267-2022>, 2022.
- 490 Tozato, K.: K-Tozato/3D_tsunami_simulation: (Dataset_for_NHESS), Zenodo [data set], <https://doi.org/10.5281/zenodo.6394294>, 2022.
- Winter, A.O., Alam, M.S., Asce, S.M., Shekhar, K., Motley, M.R., Asce, M., Eberhard, M.O., Barbosa, A.R., Asce, A.M., Lomonaco, P., Arduino, P., Cox, D.T.: Tsunami-like wave forces on an elevated coastal structure: Effects of flow shielding and channeling. *J. Waterw. Port Coast. Ocean Eng.* 146, 04020021, [https://doi.org/10.1061/\(ASCE\)WW.1943-5460.0000581](https://doi.org/10.1061/(ASCE)WW.1943-5460.0000581), 2020.
- 495 Xiong, Y., Liang, Q., Park, H., Cox, D., Wang, G.: A deterministic approach for assessing tsunami-induced building damage through quantification of hydrodynamic forces. *Coast. Eng.* 144, 1–14, <https://doi.org/10.1016/j.coastaleng.2018.11.002>, 2019.
- Zhang, W., Yun, Y.: Multi-scale accessibility performance of shelters types with diversity layout in coastal port cities: A case study in Nagoya City, Japan. *Habitat Int.* 83, 55–64, <https://doi.org/10.1016/j.habitatint.2018.11.002>, 2019.